

---

# SMA and ALMA Studies of Disk- and Planet Formation around Low-mass Protostars

---

Shigehisa Takakuwa<sup>1,2</sup>, Hsi-Wei Yen<sup>2,3</sup>, Ti-Lin Chou<sup>2,4</sup>, Nagayoshi Ohashi<sup>2,5</sup>, Yusuke Aso<sup>5,6</sup>, Patrick M. Koch<sup>2</sup>, Ruben Krasnopolsky<sup>2</sup>, Paul T. P. Ho<sup>2,7</sup>, Hanyu Baobab Liu<sup>2,3</sup>, Naomi Hirano<sup>2</sup>, Pin-Gao Gu<sup>2</sup>, Chin-Fei Lee<sup>2</sup>, Evaria Puspitaningrum<sup>8</sup>, Yuri Aikawa<sup>9</sup>, Masahiro N. Machida<sup>10</sup>, Kazuya Saigo<sup>11</sup>, Masao Saito<sup>12</sup>, Kengo Tomida<sup>13</sup>, & Kohji Tomisaka<sup>14</sup> TAKAKUWA@SCI.KAGOSHIMA-U.AC.JP

1. Department of Physics and Astronomy, Graduate School of Science and Engineering, Kagoshima University, 1-21-35 Korimoto, Kagoshima, Kagoshima 890-0065, Japan; takakuwa@sci.kagoshima-u.ac.jp; 2. Academia Sinica Institute of Astronomy and Astrophysics, P.O. Box 23-141, Taipei 10617, Taiwan; 3. European Southern Observatory, Karl-Schwarzschild-Str. 2, Garching 85748, Germany; 4. Kavli Institute for Cosmological Physics and The Enrico Fermi Institute, The University of Chicago, Chicago, IL, USA; 5. Subaru Telescope, National Astronomical Observatory of Japan, 650 North A'ohoku Place, Hilo, HI 96720, USA; 6. Department of Astronomy, Graduate School of Science, The University of Tokyo, 731 Hongo, Bunkyo-ku, Tokyo 113-0033, Japan; 7. East Asian Observatory, 660 North A'ohoku Place, Hilo, Hawaii 96720, USA; 8. Department of Astronomy, Faculty of Mathematics and Natural Sciences, Institut Teknologi Bandung, Jl. Ganesha 10, Bandung 40132, Indonesia; 9. Center for Computational Science, University of Tsukuba, Tsukuba, Ibaraki 305-8577, Japan; 10. Department of Earth and Planetary Sciences, Faculty of Sciences, Kyushu University, Fukuoka 812-8581, Japan; 11. ALMA Project Office, National Astronomical Observatory of Japan, Osawa 2-21-1, Mitaka, Tokyo 181-8588, Japan; 12. Nobeyama Radio Observatory, National Astronomical Observatory of Japan, Minamimaki, Minamisaku, Nagano 384-1805, Japan; 13. Department of Earth and Space Science, Osaka University, Machikaneyama-cho, Toyonaka-shi, Osaka 560-0043, Japan; 14. National Astronomical Observatory of Japan, Osawa, 2-21-1, Mitaka, Tokyo 181-8588, Japan

## Abstract

We report our current SMA and ALMA studies of disk and planet formation around protostars. We have revealed that  $r \gtrsim 100$  AU scale disks in Keplerian rotation are ubiquitous around Class I sources. These Class I Keplerian disks are often embedded in rotating and infalling protostellar envelopes. The infalling speeds of the protostellar envelopes are typically  $\sim 3$ -times smaller than the free-fall velocities, and the rotational profiles follow the  $r^{-1}$  profile, that is, rotation with the conserved specific angular momentum. Our latest high-resolution ( $\sim 0''.5$ ) ALMA studies, as well as the other studies in the literature, have unveiled that  $r \sim 100$ -AU scale Keplerian disks are also present in several Class 0 protostars, while in the other Class 0 sources the inferred upper limits of the Keplerian disks are very small ( $r \lesssim 20$  AU). Our recent data analyses of the ALMA long baseline data of the Class I-II source HL Tau have revealed gaps in molecular gas as well as in dust in the surrounding disk, suggesting the presence of sub-Jovian planets in the disk. These results imply that disk and planet formation should be completed in the protostellar stage.

## 1. Introduction

Two of the most intriguing astrophysical questions are when and how planets form. A classical picture is that planetary systems form out of protoplanetary disks around T-Tauri stars. Recent theoretical studies, however, predict that planets can form when the central stars are still in the protostellar (Class 0-I) phase, due to the gravitational instabilities of massive disks surrounding the protostars (Vorobyov, 2011; Tsukamoto et al., 2013; 2015). Observational investigations of disk and planet formation around protostars, however, have been difficult as they are deeply embedded within protostellar envelopes. The advent of new (sub)millimeter interferometers, SMA, and ALMA, has now enabled us to perform high-resolution and high-sensitivity observations of protostellar sources, to identify disks around protostars, and to study the formation mechanisms of disks and then planets.

We have been conducting systematic SMA and ALMA observations of protostars. Our group effort aims to unveil the time scale of planet formation, a long-standing but unresolved astrophysical question. Our perspective is that disk and planet formation will be initiated and completed during the protostellar stage and before the T-Tauri stage, as is supported by our observational results described below.

## 2. Class I

In Figure 1, SMA+ASTE images of the submillimeter CS (7–6) emission toward the Class I protostellar binary L1551 IRS 5 (contours), superposed on the SMA image of the 0.9-mm dust continuum emission (gray), are shown (Chou et al., 2015). In the high-velocity region, the blueshifted and redshifted CS emission trace the southeastern and northwestern parts of the dust-continuum emission, and exhibit a velocity gradient along the major axis of the dust-continuum emission. In contrast, in the low-velocity region the blueshifted and redshifted CS emission are extended beyond the continuum emission, and they overlap significantly. The centroid location of the blueshifted emission is slightly shifted to the south, and that of the redshifted emission to the west and northwest.

To interpret the observed velocity structures in the submillimeter CS emission, we made a simple geometrically-thin disk + envelope model. Figure 2 shows the results of the  $\chi^2$  model fitting to the high-velocity blueshifted and redshifted CS emission. Our model fitting demonstrates that the observed high-velocity CS emission is well reproduced by a geometrically-thin Keplerian-disk model with the central stellar mass  $M_\star = 0.5 M_\odot$  and the outermost radius  $R_{kep} = 64$  AU. On the other hand, the spatial-velocity distribution of the low-velocity CS emission can be modeled with a rotating and infalling envelope. The envelope rotation follows the  $v_{rot} \propto r^{-1}$  law, that is, rotation with the conserved specific angular momentum, and the angular momentum of the infalling envelope connects smoothly to that at the outermost radius of the central Keplerian disk. The infalling velocity in the envelope is a factor  $\sim 3$  slower than the free-fall velocity estimated from the central protostellar mass, which is derived from the central Keplerian rotation.

Our SMA and ALMA observations have also identified  $r \sim 100$ -300 AU scale Keplerian disks around the Class I protostars L1551 NE (Takakuwa et al., 2012; 2013; 2014; 2015; 2016), TMC-1A (Aso et al., 2015), and L1489 IRS (Yen et al., 2013; 2014). The surrounding envelopes exhibit an  $r^{-1}$  rotational profiles in TMC-1A and L1489 IRS, while no clear rotation is seen in the envelope around L1551 NE. All these protostellar envelopes show infalling motion  $\sim 3$ -times slower than the corresponding free-fall except for L1489 IRS, where the envelope consists of free-fall gas streams onto the central Keplerian disk. Table 1 summarizes these results.

## 3. Class 0

The above results, as well as the other results in the literature (Lommen et al., 2008; Brinch et al., 2013; Lindberg et al., 2014), demonstrate that Keplerian disks are ubiquitous around Class I sources. To clarify how early such Keplerian disks are formed around protostars, we have also conducted high-resolution ( $\lesssim 0''.5$ ) ALMA observations of Class 0 protostars (Yen et al., 2016b). Figure 3 shows moment 0 (contours) and 1 (colours) maps of the  $C^{18}O$  (2–1) emission toward three Class 0 protostars in the southern sky, IRAS 16253-2429, IRAS 15398-3559, and Lupus 3 MMS. While these protostars are all Class 0 protostars with low bolometric temperatures ( $T_{bol} \lesssim 60$  K), the velocity structures of their circumstellar materials differ significantly. In IRAS 16253-2429 the protostellar envelope exhibits a velocity gradient along the direction of the outflow, while in IRAS 15398-3559 velocity gradients both along and across the outflow axis are seen. In Lupus 3 MMS the northwestern and southeastern parts show blueshifted and redshifted emission, respectively, and the velocity gradient is approximately perpendicular to the outflow axis.

Figure 4 shows the observed (black contours) and model (red) Position - Velocity (P-V) diagrams of the three Class 0 protostars in the  $C^{18}O$  emission along (left panel) and across the outflow axes (right). In Lupus 3 MMS, along the major axis the blueshifted and redshifted emission are separated and located to the northwestern and southeastern parts, respectively. It is also clear that the higher-velocity emission resides closer to the central protostar. Along the minor axis no clear velocity gradient is seen, while the velocity width becomes wider near the protostellar position. Our model (red contours) shows that the observed spatial and velocity features are reproduced by a Keplerian disk with  $M_\star = 0.3 M_\odot$  and  $R_{kep} = 130$  AU. In IRAS 15398-3559, velocity gradients are seen both along and across the outflow axes. Our model reveals that these features can be interpreted by an infalling envelope with  $r^{-1}$  rotation. Toward IRAS 16253-2429, on the other hand, only the velocity gradient along the outflow axis can be identified, suggesting infall without a clear rotation.

Figure 5 shows our compilation of the central stellar masses versus the radii of the Keplerian disks ( $M_\star - R_{kep}$ ) for a sample of Class 0 and I protostars from our previous observations and from the literature. Red and blue symbols denote the results of the Class 0 and I sources, respectively. A number of Class I and several Class 0 protostars possess large ( $r \gtrsim 50$  AU) Keplerian disks, and the protostellar masses of the

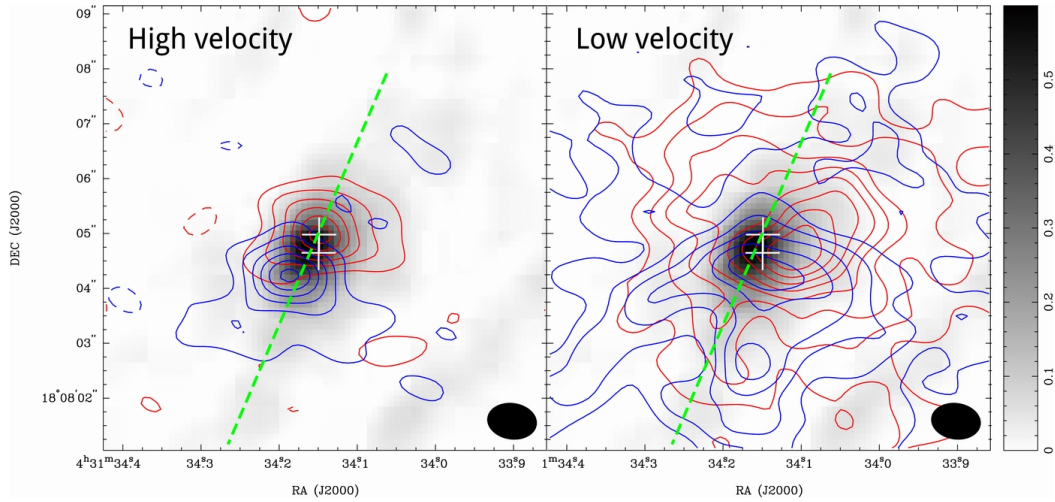


Figure 1. Distributions of the high- and low-velocity blueshifted (blue contours) and redshifted (red) CS (7-6) emission in the Class I protostar L1551 IRS 5 obtained with the SMA and ASTE, superposed on the 343 GHz continuum image (gray scale). This figure is taken from Figure 5 by Chou et al. (2014).

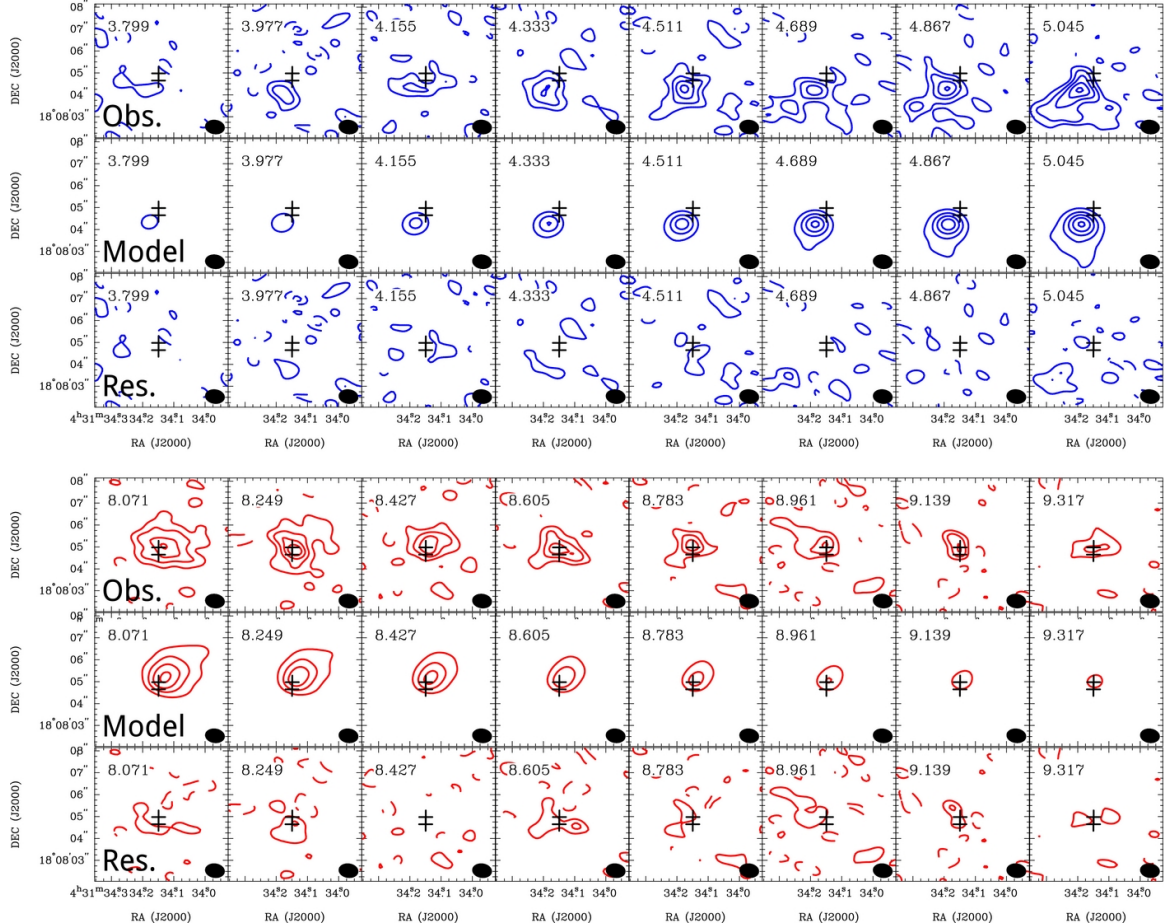


Figure 2. Best-fit results of the  $\chi^2$  model fitting of the geometrically-thin Keplerian disk to the SMA+ASTE CS (7-6) velocity channel maps in L1551 IRS 5 at the highly blueshifted (blue contours) and redshifted (red) velocities. Upper, middle, and lower panels show the observed, model, and the residual velocity channel maps, respectively, where the best-fit parameters are  $M_* = 0.5 M_\odot$ , the disk inclination angle  $i = -60^\circ$ , and the disk position angle  $\theta = -33^\circ$ , respectively. This figure is taken from Figure 7 by Chou et al. (2014).

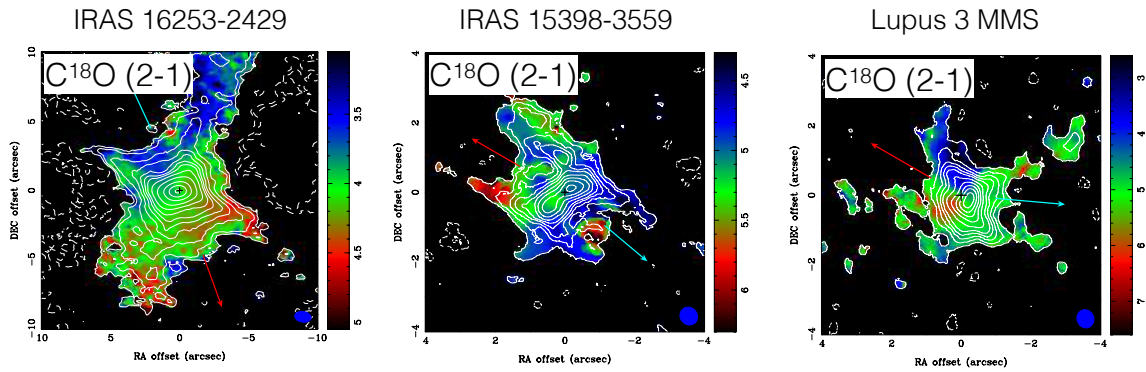


Figure 3. Moment 0 (white contours) and 1 maps (colors) of the  $C^{18}O$  (2–1) emission toward three Class 0 protostars observed with ALMA. Crosses denote the positions of the protostars, and blue and red arrows the directions of the blueshifted and redshifted outflows, respectively. This figure is taken from Yen et al. (2017).

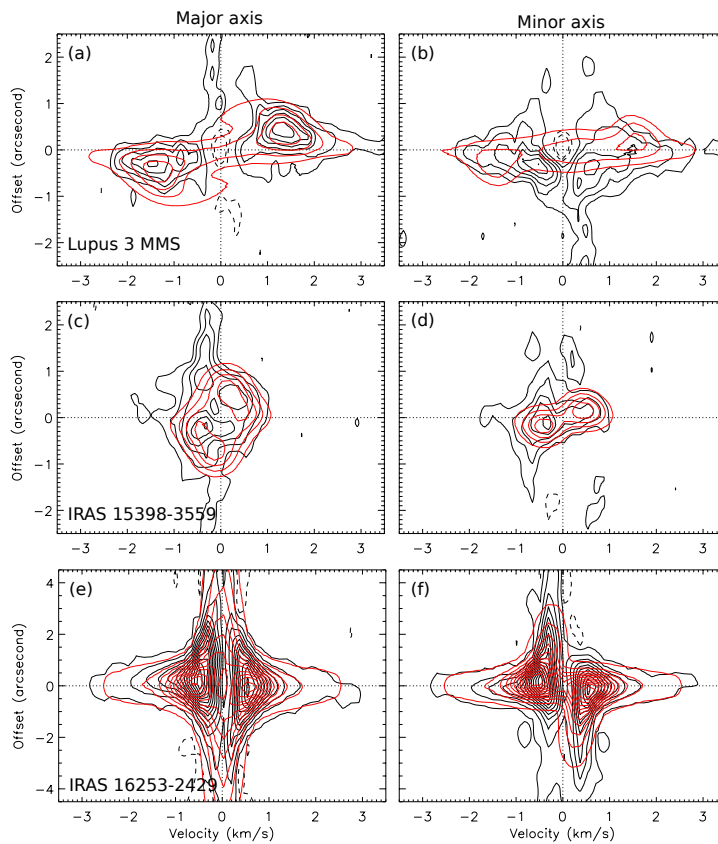


Figure 4. Observed (black contours) and model (red) Position-Velocity (P-V) diagrams of the  $C^{18}O$  (2–1) emission toward the three Class 0 protostars along the major and minor axes of the protostellar envelopes. This figure is taken from Yen et al. (2017).

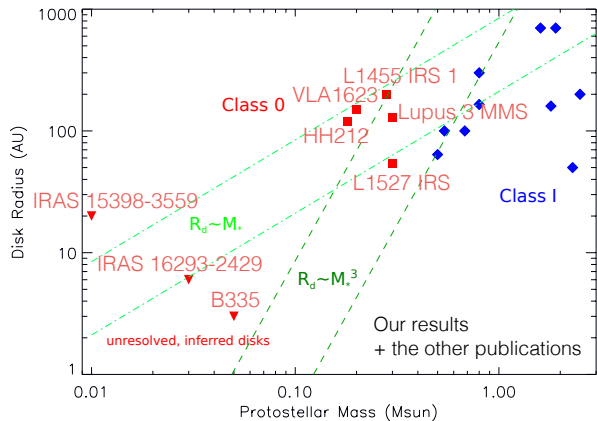


Figure 5. Plots of the protostellar masses versus the outermost radii of the Keplerian disks for a sample of Class 0 and I protostars. Red squares and blue diamonds present Class 0 and I protostars associated with the resolved Keplerian disks. Red downward triangles denote the Class 0 protostars without direct detections of the Keplerian disks. Their inferred protostellar masses and disk radii are upper limits. Dark and light green lines denote the scaling relations between protostellar masses and disk radii in the collapse models by Terebey et al. (1984) and Basu (1998), respectively. This figure is taken from Yen et al. (2017).

Class 0 sources are systematically lower than those of the Class I sources. Besides, there is another group of Class 0 protostars (IRAS 15398-3559, IRAS 16293-2429, and B335) with very small upper limits of the Keplerian radii ( $\lesssim 20$  AU) and the protostellar masses ( $\lesssim 0.05 M_{\odot}$ ). These results imply that the formation of  $r \sim 100$  AU scale Keplerian disks should be completed by the late Class 0 stage ( $\sim 10^5$  yr).

#### 4. HL Tau

As discussed above, disk formation around protostellar sources is likely to be completed by the beginning of the Class I phase. Thus, planet formation may be initiated from as early as the Class I stage. A famous Class I-II source as a candidate of planet formation is HL Tau (Dipierro et al., 2015; Kanagawa et al., 2015), where ALMA partnership et al. (2015) have identified seven ringlike gaps in the disk as seen in the dust-continuum emission. The gaps in the dust-continuum emission, however, can be created by spatial variations of dust properties and they do not necessarily reflect the “real” gaps of material (Zhang et al., 2015; Okuzumi et al., 2016). To reveal whether the dust gaps are real material gaps or not and to discuss whether planet formation is indeed ongoing in the disk, it is critical to observe the distribution of the 100

times more abundant molecular gas.

Signal-to-noise ratios of molecular-line images are generally much lower than those of dust-continuum images, because molecular-line images cannot have wide bandwidths. The lower signal-to-noise ratios result in limited spatial resolutions of the molecular-line images. To overcome these problems and to unveil the corresponding gaps of molecular lines in the disk around HL Tau, we made a high-resolution ( $\sim 0''.1 \times 0''.05$ )  $\text{HCO}^+$  (1–0) image cube from the same ALMA dataset as that of the dust gaps, and performed annular averaging of the  $\text{HCO}^+$  image cube (Yen et al., 2016a). While the annular averaging loses the azimuthal information, it can produce a high-resolution and high-sensitivity radial intensity profile, as shown in Figure 6. The derived radial profile of  $\text{HCO}^+$  clearly exhibits two gaps at radii of  $\sim 28$  AU (*c.f.*, orbital radius of Neptune = 30 AU) and  $\sim 69$  AU, which correspond to the locations of the dust gaps of D2 and D6. The FWHM widths of the inner and outer  $\text{HCO}^+$  gaps are both estimated to be  $\sim 14$  AU, and the depths are estimated to be a factor  $\sim 2.4$  and  $\sim 5.0$ , respectively. The presence of the two gas gaps in the inner two dust gaps implies that these two gaps are real gaps of material. The most interesting interpretation is that these gaps trace orbits of planet bodies which are sweeping material along their orbits, although secular gravitational instability can also create such gaps (Takahashi & Inutsuka, 2014). From the observed widths and depths of the inner and outer gaps, the masses of the putative planet bodies are estimated to be  $\sim 0.8 M_J$  and  $\sim 2.1 M_J$ , respectively (Kanagawa et al., 2015).

These results imply that planet formation can be initiated from as early as the Class I stage. Our group has an approved follow-up ALMA project to directly measure the gas gaps without the annular averaging in the higher- $J$   $\text{HCO}^+$  transitions, and ALMA and ACA data of the envelope surrounding the HL Tau disk. With these data we will continue to study the details of the planet-forming system.

#### 5. Summary

We have been conducting SMA and ALMA studies of disk- and planet formation around protostars. We consider that disk and planet formation should be completed within the protostellar phase. If our working hypothesis could be proven observationally, this should impact our understanding of planet formation significantly. So far, we have obtained the following results, which are indeed supporting our hypothesis.

1.  $r \gtrsim 100$  AU-scale Keplerian disks are ubiquitous

Table 1. Summary of our SMA and ALMA Observations of Protostellar Sources

Protostar	$T_{bol}$ (K)	$M_*$ ( $M_\odot$ )	Envelope	$R_{kep}$ (AU)	Our Publications
Class 0					
B335	31	0.05	Infall, Slow Rotation	<3	Yen et al. 2010; 2011; 2013; 2015a,b
IRAS 16293-2429	36	0.03	Infall, Slow Rotation	<6	Yen et al. 2017
Lupus 3 MMS	39	0.3	Keplerian Disk only	130	Yen et al. 2017
L1527 IRS	59	0.3	Slow Infall, $r^{-1}$ Rotation	54	Yen et al. 2013; 2015a; Ohashi et al. 2014
IRAS 15398-3559	61	0.01	Infall, $r^{-1}$ Rotation	<20	Yen et al. 2017
Class I					
L1551 NE	91	0.8	Slow Infall, Slow Rotation	300	Takakuwa et al. 2012; 2013; 2014; 2015; 2016
L1551 IRS 5	92	0.5	Slow Infall, $r^{-1}$ Rotation	64	Takakuwa et al. 2004; Chou et al. 2014
TMC-1A	172	0.64	Slow Infall, $r^{-1}$ Rotation	100	Yen et al. 2013; Aso et al. 2015
L1489 IRS	238	1.6	Freefall, $r^{-1}$ Rotation	300	Yen et al. 2013; 2014

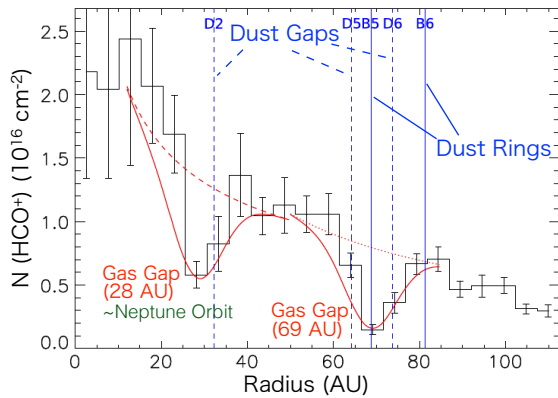


Figure 6. Radial profile of the  $\text{HCO}^+$  column density in the protoplanetary disk around HL Tau. Histograms with the error bars denote the observed values. Red dashed and dotted lines present the fitted power-law profiles outside the inner and outer gaps, respectively, and red solid lines delineate the observed gaps. This figure is taken from Yen et al. (2016a).

around Class I protostars. Such disks are also seen in several Class 0 protostars, while in the other Class 0 protostars the upper limits of the Keplerian radii are very small ( $r \lesssim 20$  AU). Thus, there is an apparent bimodality of Keplerian radii among the Class 0 samples. These results indicate rapid growth of Keplerian disks during the short Class 0 stage ( $\sim 10^5$  yr).

- Those protostellar sources, both with and without large Keplerian disks, are often embedded in infalling envelopes. In many sources the infalling envelopes also exhibit rotating motions, and the rotational profiles follow the  $r^{-1}$  profile, that is, rotation with conserved specific angular momentum. The angular momentum of the infalling envelope connects smoothly to that at the outermost radius of the central Keplerian disk. On the other

hand, the infalling velocity is a factor  $\sim 3$  slower than the free-fall velocity estimated from the central protostellar mass, which is derived from the central Keplerian rotation.

- We have re-analyzed the ALMA long baseline data of HL Tau in the  $\text{HCO}^+$  (1–0) emission. With the annular averaging, we have made a high-resolution ( $\sim 10$  AU) radial profile of the  $\text{HCO}^+$  column density, and have found two regions deficient of molecular gas (“gaps”) at radii of  $\sim 28$  AU and  $\sim 69$  AU, which are consistent with the locations of the dust gaps. These results imply that these two gaps of molecular gas and dust are real gaps of material. The FWHM widths of the inner and outer  $\text{HCO}^+$  gaps are both estimated to be  $\sim 14$  AU, and the depths are estimated to be a factor  $\sim 2.4$  and  $\sim 5.0$ . Assuming that these gaps are created by planetary bodies, the inferred planet masses are  $\sim 0.8 M_J$  and  $\sim 2.1 M_J$  at radii of 28 and 69 AU, respectively.

## Acknowledgments

S.T. and P.M.K. acknowledge grants from the Ministry of Science and Technology (MOST) of Taiwan (MOST 102-2119-M-001-012-MY3) and (MOST 103-2119-M-001-009), respectively. S.T. is grateful to a grant JSPS KAKENHI Grant Number JP16H07086, in support of this work. This paper makes use of the following ALMA data: ADS/JAO.ALMA#2013.1.00879.S and ADS/JAO.ALMA#2011.0.00015.SV. ALMA is a partnership of ESO (representing its member states), NSF (USA) and NINS (Japan), together with NRC (Canada) and NSC and ASIAA (Taiwan), in cooperation with the Republic of Chile. The Joint ALMA Observatory is operated by ESO, AUI/NRAO and NAOJ.

## References

- ALMA Partnership, Brogan, C. L., Pérez, L. M., *et al*, ApJ, 808, L3, 2015.
- Aso, Y., Ohashi, N., Saigo, K., *et al*, ApJ, 812, 27, 2015.
- Basu, S., ApJ, 509, 229, 1998.
- Brinch, C., & Jørgensen, J. K., A&A559, A82, 2013.
- Chou, T.-L., Takakuwa, S., Yen, H.-W., Ohashi, N., & Ho, P. T. P., ApJ, 796, 70, 2014.
- Dipierro, G., Price, D., Laibe, G., *et al*, MNRAS, 453, L73, 2015.
- Kanagawa, K. D., Muto, T., Tanaka, H., *et al*, ApJ, 806, L15, 2015.
- Lindberg, J. E., Jørgensen, J. K., Brinch, C., *et al*, A&A, 566, A74, 2014.
- Lommen, D., Jørgensen, J. K., van Dishoeck, E. F., & Crapsi, A., A&A, 481, 141, 2008.
- Ohashi, N., Saigo, K., Aso, Y., *et al*, ApJ, 796, 131, 2014.
- Okuzumi, S., Momose, M., Sirono, S., *et al*, ApJ, 821, 82, 2016.
- Takakuwa, S., Ohashi, N., Ho, P. T. P., *et al*, ApJ, 616, L15, 2004.
- Takakuwa, S., Saito, M., Lim, J., *et al*, ApJ, 754, 52, 2012.
- Takakuwa, S., Saito, M., Lim, J., & Saigo, K., ApJ, 776, 51, 2013.
- Takakuwa, S., Saito, M., Saigo, K., *et al*, ApJ, 796, 1, 2014.
- Takakuwa, S., Kiyokane, K., Saigo, K., & Saito, M., ApJ, 814, 160, 2015.
- Takakuwa, S., Saigo, K., Matsumoto, T., *et al*, ApJ, submitted, 2016.
- Takahashi, S. Z., & Inutsuka, S.-I., ApJ, 794, 55, 2014.
- Terebey, S., Shu, F. H., & Cassen, P., ApJ, 286, 529, 1984.
- Tsukamoto, Y., Machida, M. N., & Inutsuka, S., MNRAS, 436, 1667, 2013.
- Tsukamoto, Y., Takahashi, S. Z., Machida, M. N., & Inutsuka, S., MNRAS, 446, 1175, 2015.
- Vorobyov, E. I., ApJ, 729, 146, 2011.
- Yen, H.-W., Takakuwa, S., & Ohashi, N., ApJ, 710, 1786, 2010.
- Yen, H.-W., Takakuwa, S., & Ohashi, N., ApJ, 742, 57, 2011.
- Yen, H.-W., Takakuwa, S., Ohashi, N., & Ho, P. T. P., ApJ, 772, 22, 2013.
- Yen, H.-W., Takakuwa, S., Ohashi, N., *et al*, ApJ793, 1, 2014.
- Yen, H.-W., Koch, P. M., Takakuwa, S., *et al*, ApJ, 799, 193, 2015a.
- Yen, H.-W., Takakuwa, S., Koch, P. M., *et al*, ApJ, 812, 129, 2015b.
- Yen, H.-W., Liu, H. B., Gu, P.-G., *et al*, ApJ, 820, L25, 2016a.
- Yen, H.-W., Koch, P. M., Takakuwa, S., *et al*, ApJ, 834, 178, 2017.
- Zhang, K., Blake, G. A., & Bergin, E. A., ApJ, 806, L7, 2015.